RESEARCH ARTICLE

Gravity Modulation Analysis of Heat Transfer and Magnetic Boundary Layer of MHD Fluid Along Vertical Plate with Variable Viscosity and Porous Medium Effects

Zia Ullah[1,*], Amir Abbas[2], Uzma Tariq[1], Malik Izhar Ul Haq[1], Alishba Kaynat[1], Anila Bibi[1], Tehreem Soha[1], M Waheed Iqbal[1] and Muhammad Ashraf[1]

[1] Department of Mathematics and Statistics, The University of Lahore, Sargodha-Campus, 40100 Sargodha, Pakistan
[2] Department of Mathematics, Faculty of Natural Science and Technology, Baba Guru Nanak University, Nankana Sahib 39100, Pakistan

Abstract

The magnetic fluid flow through vertical surface plays a significant impact in engineering and industrial processes of insulating materials and heat exchangers. The main theme of this mechanism is to obtain the heat and magnetic flux of viscous fluid motion along the symmetrical magnetized surface with variable viscosity, porous medium and magneto-hydrodynamic effects. The goal of present numerical research is to find the stability in thermal management of vertical magnetic plates in manufacturing processes. The mathematical analysis is performed by using stream functions and similarity variables for smooth coding in MATLAB program. The convenient form of present model is derived by using the combined relation of Keller box and Newton Raphson approach under defined boundary values along the magnetized plate. The fluid velocity, heat transfer and magnetic flux are the main findings of this wok. It is depicted that fluid velocity and temperature profile enhances for small viscosity and maximum reduced gravity. It is exhibited that temperature profile enhances as Prandtl number and porous medium enhances. It is found that heat transport and magnetic flux enhances as reduced gravity enhances. It is also noticed that skin friction and magnetic flux performs opposite behavior for maximum values of porous medium.

Keywords: magnetohydrodynamic, reduced gravity, variable viscosity, porous medium, magnetic flux, heat transport.

1 Introduction and Literature Review

The prominent importance of current mechanism is to check the magnetic driven fluid motion along the vertical porous plate with porous medium, variable viscosity, reduced gravity and magnetic field effects. The movement of an insoluble viscous fluid and the transmission of heat characteristics across a plate have

Submitted: 27 March 2025
Accepted: 04 August 2025
Published: 15 August 2025

Vol. 1, **No.** 2, 2025.
10.62762/CEHT.2025.812351

***Corresponding author:**
✉ Zia Ullah
ziakhan6009@gmail.com

Citation
Ullah, Z., Abbas, A., Tariq, U., Haq, M. I. U., Kaynat, A., Bibi, A., Soha, T., Iqbal, M. W., & Ashraf, M. (2025). Gravity Modulation Analysis of Heat Transfer and Magnetic Boundary Layer of MHD Fluid Along Vertical Plate with Variable Viscosity and Porous Medium Effects. *Computational Environmental Heat Transfer*, 1(2), 51–64.

gained a lot of interest in recent years due to their multiple useful uses in biochemical and methods of production. Mixed convection boundary layer movements of viscid non-compressible liquid are gaining popularity as a result of their multiple useful uses in industries and production. The technique is helpful for exchanging heat, researching sunspots, constructing ballistic missiles, investigating how substances flow in the universe, manipulating fluids such as metallic substances, cooled nuclear energy plants, managing bloodstream fluid, and investigating Earth science and aerospace. Kay et al. [1] studied the thermal bar boundary-layer analysis for heat transfer with reduced gravity effects numerically. They discovered that for lower Nusselt number, the thermal boundary layer is thicker. Hazrika et al. [2] deduced the impacts of thermal-conductivity and viscosity on MHD flow past an upward plate with the help of shooting method numerically. They observed the impact of viscosity parameter on concentration profile prominently. The effect of changing characteristics and thermophoresis on free force convective flow along a vertical cylinder in a porous media was investigated by Srinivasacharya et al. [3]. The impact of viscosity and varying thermal conductivity on boundary layer MHD along a vertical surface was examined by Gbadeyan et al. [4]. They observed that when the magnetic parameter became stronger, the velocity profile decreased. Using the finite difference approach, Chin et al. [5] conducted a computational investigation of the effects of varying viscosity on free force convection boundary layer flow across a vertical cylinder implanted in a porous medium. They discovered that the linear relationship between fluid viscosity and temperature is inverse. Mahmoud [6] investigated the effect of the chemical reactions and heat production on dual diffusive heat transfer across a non-isothermal horizontal shape in a porous medium of changing viscosity. They discovered that the viscosity parameter raises the local Sherwood and Nusselt numbers. The effect of change in viscosity and thermal conductivity on free force convection dissipative viscose fluid flow across a rotating geometry was examined by Malik et al. [7]. They found that the velocity profile is decreased for large value of unsteady parameter.

In all the previous studies, they thought that the thickness of the fluid and the pull of gravity stayed the same as the temperature at the edge of the fluid layer changed. But in reality, when the fluid gets heated up from the inside, its properties change a lot. The temperature makes a big difference in how thick the fluid is and how strong gravity pulls on it. Normally, when liquids get hotter, they become less thick, but with gases, they get thicker as they get hotter. Elaiw et al. [8] developed a numerical analysis under the influence of viscosity on the vertex-flow instability for non-Darcy mixed convective mechanism along the non-isothermal in porous medium. Hazarika et al. [9] presented the numerical and experimental phenomenon with viscosity and MHD mixed convective mechanism along heated geometry with the help of shooting method. They found a decrease in velocity due to increasing value of viscosity parameter. Lin et al. [10] computed a computational mechanism of mixed convective mechanism along heated geometry in the presence of thermally satisfaction medium. Kishan et al. [11] considered a flow analysis with viscosity impact on free force convective over a semi-infinite upward porous geometry numerically. Pullepu et al. [12] developed a computational framework for free convective movement along an upward shape that accounts for both energy production and chemical interactions. On free forced convection flow along porous geometry, Abbas et al. [13] reported the combined effect of thermophoretic motion and changing viscosity. In order to understand how varying viscosity and thermal conductivity affect steady mixed convection flow of incompressible fluid along a vertical form, Umavathi et al. [14] conducted an analysis. Pullepu et al. [15] quantitatively studied the effects of free convection movement through a horizontal design, including generated heat and chemical-based reaction. Palani et al. [16] solved numerically and analyzed the theoretical solution for the free convective problem on a vertical geometry with thermal-conductivity and variable viscosity. Reddy et al. [17] worked extensively on the study of porosity and variable viscosity of the fluid for combined effect of Soret and Dafour by using shooting method.

The researchers in [18] constructed heat and mass flux phenomenon on MHD mixed convective flow of an incompressible viscous flow numerically by using first order chemical reaction. They noticed that velocity and chemical reaction parameter are inversely proportional to each other. Srinivasacharya et al. [19] investigated a numerical simulation of radiation impact on free force convective due to vertical wavy-shape in porous material. Authors [20–23] investigated the effects of transverse magnetic

field, chemical reaction, porous medium, and natural convection on heat and mass transfer over various surfaces. The effects of non-uniform heat generation, porous medium, thermal radiations and MHD on heat transfer over confined cylinder was examined in reference [24]. The optimization of flow dynamics, thermal rate and mass flow over stretched surface with inclined magnetic field was solved through numerical methods in reference [25]. Bayones et al. [26] analyzed the heating optimization and mass flow of mass and thermal rate in a tube using fractional Maxwell fluid. Reduced gravity impact on free convective heat transfer from a finite flat vertical plate was studied by Lotto et al. [27]. The numerical and experimental convection phenomena under low gravity, which are important in space material processing, were presented by ostarch [28]. Laminar convection promotes separation, and thermo solutal convection at reduced gravity appears to be a promising and advantageous occurrence according to the researchers. The impacts of hybrid nanoparticles and buoyancy force on convective heat transfer of gravity driven fluid flow along vertical plane structure were investigated by Awwad et al. [29]. Maranna et al. [30] Studied the movement of material through mass transpiration with the effects of magnetohydrodynamics and radiation on thick fluid flowing past an elongated form. Mabood et al. [31] explored the behaviors of Jeffrey nanofluid involving entropy and magnetohydrodynamics effects on a stretched shape, considering various engineering uses. The influence of heat source, convective boundaries, MHD, chemical reaction, nanoparticles, and inclined magnetic field on heat and mass flow of fluid over various structures was explored [32–37].

They found that all the studies mentioned earlier focused on a small temperature gap among surface liquid and surrounding liquid. The temperature difference is very large in some thermodynamic flows. In such cases, the Boussinesq approximation is not suitable anymore (see Key [1]). To deal with these situations, the idea of using temperature-related changes in gravity and thickness of the fluid is proposed in [1]. This is meant for situations where there's a big difference in temperature. The research investigates how heat and magnetic strength work on a vertical magnetic porous plate. They use an idea from a previous study [1] and look at how changes in fluid thickness due to temperature and the pull of gravity affect the movement of electrically-conductive fluid. The study uses computer calculations to understand this. They use a method called the Keller Box method to solve the equations, and then they use software called MATLAB to make graphs and numbers. These graphs show things like how fast the fluid is moving, how strong the magnetic field is, and how hot it is. They also look at the slopes of these graphs, which tell us about things like how the fluid rubs against the plate, how heat is transferred, and how strong the magnetic power is. This helps them understand how things change along the plate. The main research gap between present and existing literature is to predict heat transfer rate under variable gravity not constant gravity. In reduced gravity, the gravitational acceleration depends on maximum temperature and maximum density effects which present significant relation due to temperature. In this study, the combined effects of MHD, temperature dependent viscosity and reduced gravity on magnetized fluid for heat transfer performance were explored.

2 Flow problem and mathematical description

This research is dedicated to numerically solving a magneto-thermo analysis problem, considering temperature-dependent gravity and viscosity for convective heat transfer around a magnetized heated shape embedded in porous material. The problem will be transformed into a set of nonlinear models, which will then be converted in suitable form applying the stream-function approach. The modified model is tackled applying Finite Difference Method (FDM) combined with the Keller/Box technique. The computational results, based on the specified pertinent parameters, will be presented in both geometrical and statistical formats.

We're exploring a scenario involving a steady, two-dimensional, and non-compressible electrically conducting liquid. We're observing velocity fields u and v along the x and y directions in Figure 1. H_x and H_y represents the magnetism intensities in those directions, with $H_x = H_0$ at the surface, where H_0 is the magnetic field strength.

In the literature, most studies assume constant fluid properties. However, under specific circumstances, especially the fluid viscosity can change with temperature. This can be expressed mathematically as $\mu = \mu_\infty[1 + \gamma(T - T_\infty)]$ by following [2, 4, 5, 8, 9]. The following equations depict the expressions for continuity, momentum, magnetic force, and energy:

$$\frac{\partial u}{\partial x} + \frac{\partial v}{\partial y} = 0 \tag{1}$$

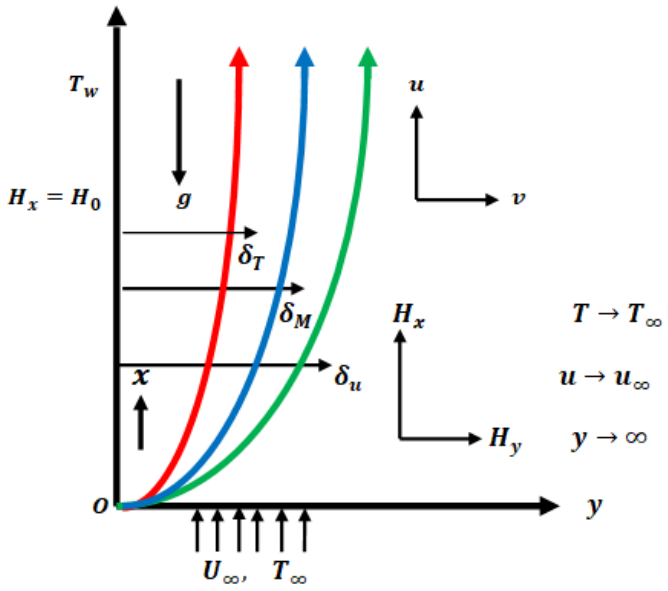

Figure 1. Vertical plate with induced magnetic field.

$$\frac{\partial H_1}{\partial x} + \frac{\partial H_2}{\partial y} = 0 \tag{2}$$

$$u\frac{\partial u}{\partial x} + v\frac{\partial u}{\partial y} = \frac{1}{\rho}\frac{\partial}{\partial y}\left(\mu\frac{\partial u}{\partial y}\right) - \frac{\nu}{K}u + g\left(\frac{\rho-\rho_\infty}{\rho_\infty}\right) + \frac{\mu_0}{4\pi\rho}\left(H_1\frac{\partial H_1}{\partial x} + H_2\frac{\partial H_1}{\partial y}\right) \tag{3}$$

$$u\frac{\partial H_1}{\partial x} + v\frac{\partial H_1}{\partial y} = \eta\frac{\partial^2 H_1}{\partial y^2} + \left(H_1\frac{\partial u}{\partial x} + H_2\frac{\partial u}{\partial y}\right) \tag{4}$$

$$u\frac{\partial T}{\partial x} + v\frac{\partial T}{\partial y} = \frac{\kappa}{\rho C_p}\frac{\partial}{\partial y}\left(\frac{\partial T}{\partial y}\right) \tag{5}$$

The relationship between density and temperature is as follows when the temperature is sufficiently close to T_m:

$$\frac{\rho-\rho_m}{\rho_m} = -\gamma\left(T-T_m\right)^2, \quad T \to T_m \pm \Delta T \quad \text{as} \quad y \to \pm\infty \tag{6}$$

for a certain fixed ΔT. Consider region $y \geq 0$ subject to the boundary constraints in order to obtain the symmetry in this case. Where $T_\infty = T_m + \Delta T$ is related to by equation (6) and has the formula $T_\infty = T_m + \Delta T$. The reduced gravity can be easily defined as $g' = g(\frac{\rho-\rho_\infty}{\rho_\infty})$ (i.e., the fluid particles of acceleration with density ρ_m) by following [1, 24, 27, 28]. Equation (6) then becomes,

$$g' = g\gamma\frac{\rho_m}{\rho_\infty}(T_\infty - T_m)^2 \tag{7}$$

Defined boundary values are listed below;

$$u = 0; \quad v = 0; \quad H_1 = H_0, \quad H_2 = 0; \quad T = T_m \quad \text{at} \quad y = 0 \tag{8}$$

$$U \to U_\infty, \quad T \to T_\infty, \quad H_1 \to 0 \quad \text{as} \quad y \to \infty. \tag{9}$$

The appropriate limiting values of velocity/temperature, considering temperature-based viscosity, reduced gravity, and the presence of porous medium components, have been explained well. The terms $R_e x = \frac{U_\infty x}{\nu}$, U_∞, $T_m = T_\infty + \frac{T_o}{x}$, T_∞, $D = D_{axR_{ex}}$, T_o signify Reynolds parameter, free velocity, variable maximum temperature, ambient temperature, porosity medium and constant temperature over heated vertical surface.

3 Stream Variables and Similarities

The equation (10) presents stream and similarity functions to convert main model into ODEs. These ODEs show pertinent parameters which displays important role for numerical solutions.

$$u = \frac{\partial\psi}{\partial y}, \quad v = \frac{\partial\psi}{\partial x}, \quad H_1 = \frac{\delta\varphi}{\delta y}, \quad H_2 = \frac{\delta\varphi}{\delta x}, \quad \theta = \frac{T-T_\infty}{T_w - T_\infty}. \tag{10}$$

The streaming functions ϕ and ψ represent MHD flow and fluid flow behavior respectively, while θ denotes the dimensionless heat/temperature. The similarities are listed below.

$$\eta = \sqrt{\frac{u_\infty}{\nu x}}y, \quad \psi = \sqrt{u_\infty \nu x}f(\eta), \tag{11}$$

$$\varphi = \frac{H_0}{U_\infty}\sqrt{\nu x U_\infty}g, \quad T = T_\infty + \frac{T_0}{x}\theta(\eta), \quad \mu = \mu_\infty\left[1+\gamma\left(T-T_\infty\right)\right]. \tag{12}$$

Applying equations (10)-(12) to equations (1)-(5) and (8) results in the transformed non-linear ordinary differential equations (ODEs);

$$(1+\varepsilon\theta)f''' + \epsilon\theta' f'' + \frac{1}{2}f'f'' - \Omega f' + R_g\left(2\theta - \theta^2\right)\lambda - \frac{1}{2}Mgg'' = 0 \tag{13}$$

$$-\frac{fg''}{2} = P_m g''' - \frac{gf''}{2} \tag{14}$$

$$P_r\left(-\theta f' - \frac{\theta' f}{2}\right) = \theta'' \tag{15}$$

In above reduced model, the parameters $\Pr = \frac{\nu}{\alpha}$, $P_m = \frac{\eta}{\nu}$, $M = \frac{H_0^2 L^2 \mu_0}{\nu^2 4\pi\rho}$, $\lambda = \frac{g\beta^* T_0}{U_\infty^2}$, η, θ, $\Omega = \frac{1}{R_{ex}D_{ax}}$, $\epsilon = \gamma_1\left(T_m - T_\infty\right)$, γ_1, $R_g = \frac{g'}{g\beta^*\Delta T}$ present Prandtl factor, MHD Prandtl factor, magnetic parameter, convective parameter, similarity factor, unitless temperature, porosity factor, viscosity parameter, viscosity constant, and reduced gravity. The limiting values are listed below.

$$f' = 0, \quad f = 0, \quad g = 0, \quad \theta = 1, \quad g' = 1 \quad \text{at} \quad \eta = 0 \tag{16}$$

$$f' \to 1, \quad \theta \to 0, \quad g' \to 0, \quad \text{at} \quad \eta \to \infty. \tag{17}$$

The terms $Cf_x = \frac{\tau_w}{\rho {U_\infty}^2}$, $Nu_x = \frac{xq_w}{\kappa(T_w - T_\infty)}$ and $Mg_x = \frac{xj_w}{\rho {U_\infty}^2}$ present skinfriction coefficient, Nusselt coefficient and magnetic flux coefficient. The formula of τ_w, q_w and j_w are listed below.

$$\tau_w = \mu\left(\frac{\partial u}{\partial y}\right)_{y=0}, \quad q_w = -\kappa\left(\frac{\partial T}{\partial y}\right)_{y=0}, \quad j_w = \mu\left(\frac{\partial H}{\partial y}\right)_{y=0} \tag{18}$$

The main reduced form of skinfriction, Nusselt factor and magnetic flux factor is listed below.

$$\begin{aligned} {R_{e_x}}^{1/2} C_{f_x} &= f''(0), \quad {R_{e_x}}^{-1/2} N_{u_x} = -\theta'(0), \\ {R_{e_x}}^{-1/2} Mg_x &= g''(0). \end{aligned} \tag{19}$$

4 Numerical Analysis and Computational Method

The current nonlinear ordinary model is very complex and analytical solution is not easy. For this high coupled model, the numerical approximation is only possible. For this analysis, the appropriate variables are assumed in equation (20). These variables convert the high derivatives to single derivative.

$$\begin{aligned} &f' = p, \quad f'' = p' = q, \quad f''' = q', \quad g' = u, \\ &g'' = u' = v, \quad g''' = v', \quad \theta' = l, \quad \theta'' = l' = m. \end{aligned} \tag{20}$$

Equations (13)-(16) are simplified to overcome the challenges they pose. The resulting simpler forms are as follows:

$$f' = p \Rightarrow f' - p = 0 \tag{21}$$

$$p' = q \Rightarrow p' - q = 0 \tag{22}$$

$$g' = u \Rightarrow g' - u = 0 \tag{23}$$

$$u' = v \Rightarrow u' - v = 0 \tag{24}$$

$$\theta' = l \Rightarrow \theta' - l = 0 \tag{25}$$

$$(1+\epsilon\theta)q' + \epsilon l q' + \frac{1}{2}pq - \Omega p + R_g(2\theta - \theta^2)\lambda - \frac{1}{2}Mgv = 0 \tag{26}$$

$$P_m v' + \frac{fv}{2} - \frac{gq}{2} = 0 \tag{27}$$

$$m + P_r\left(\theta P + \frac{lf}{2}\right) = 0 \tag{28}$$

The ordinary form of boundary limits is listed below.

$$f = 0, \quad g = 0, \quad p = 0, \quad u = 1, \quad \theta = 1, \quad \text{at} \quad \eta = 0, \tag{29}$$

$$p \to 1, \quad u \to 0, \quad \theta \to 0, \quad \text{as} \quad \eta \to \infty. \tag{30}$$

Now using backward, central η_{n-1}, η_n and mid-point $\eta_{n-\frac{1}{2}}$ formulas of FDM scheme with initial conditions by using equations (31), we have,

$$\eta_0 = 0, \quad \eta_n = \eta_{n-1} + h_n, \quad \eta_n = \eta_\infty. \tag{31}$$

The first differential form and single function of FDM scheme are listed below in equation (32).

$$f' = \frac{f_n - f_{n-1}}{h_n}, \quad f = \frac{f_n + f_{n-1}}{2} = f_{n-\frac{1}{2}}, \tag{32}$$

and

$$f_n - f_{n-1} - \frac{1}{2}h_n\left(p_n + p_{n-1}\right) = 0, \tag{33}$$

$$p_n - p_{n-1} - \frac{1}{2}h_n\left(q_n + q_{n-1}\right) = 0, \tag{34}$$

$$g_n - g_{n-1} - \frac{1}{2}h_n(u_n + u_{n-1}) = 0, \tag{35}$$

$$u_n - u_{n-1} - \frac{1}{2}h_n\left(v_n + v_{n-1}\right) = 0, \tag{36}$$

$$\theta_n - \theta_{n-1} - \frac{1}{2}h_n(l_n + l_{n-1}) = 0, \tag{37}$$

Using the equations (33)-(37) mentioned earlier, the governing equations (21)-(30) transform into:

$$\begin{aligned}&\frac{1}{h_n}(q_n - q_{n-1}) + \frac{\varepsilon}{2h_n}(\theta_n+\theta_{n-1})(q_n - q_{n-1})\\ &+ \frac{\varepsilon}{4}(l_n + l_{n-1})(q_n + q_{n-1}) + \frac{1}{8}(p_n + p_{n-1})(q_n + q_{n-1})\\ &- \frac{\Omega}{2}(p_n + p_{n-1}) + R_g\lambda\left[(\theta_n+\theta_{n-1})\left(\frac{\theta_n+\theta_{n-1}}{2}\right)^2\right]\\ &- \frac{M}{8}(g_n + g_{n-1})(v_n + v_{n-1}) = 0\end{aligned} \tag{38}$$

$$\begin{aligned}&\frac{1}{8}\left(f_n + f_{n-1}\right)\left(v_n + v_{n-1}\right) + \frac{P_m}{h_n}\left(v_n - v_{n-1}\right)\\ &- \frac{1}{8}\left(g_n + g_{n-1}\right)\left(q_n + q_{n-1}\right) = 0\end{aligned} \tag{39}$$

$$\begin{aligned}&\frac{1}{4}\left(\theta_n + \theta_{n-1}\right)\left(P_n + P_{n-1}\right) + \frac{1}{8}\left(l_n + l_{n-1}\right)\left(f_n + f_{n-1}\right)\\ &+ \frac{1}{P_r}\left(m_n + m_{n-1}\right) = 0\end{aligned} \tag{40}$$

along with boundary conditions

$$f_0 = 0, \quad g_0 = 0, \quad P_0 = 0, \quad u_0 = 1, \quad \theta_0 = 1, \quad \text{at} \quad \eta = 0 \tag{41}$$

$$p_n \to 1, \quad \theta_n \to 0, \quad u_n \to 0, \quad \text{as} \quad \eta \to \infty \tag{42}$$

Utilizing the iterative Newton-Raphson method outlined below for a seamless algorithm;

$$f_n^{k+1} = f_n^k + \delta f_n^k, \quad p_n^{k+1} = p_n^k + \delta p_n^k \tag{43}$$

$$q_n^{k+1} = q_n^k + \delta q_n^k, \quad \theta_n^{k+1} = \theta_n^k + \delta\theta_n^k \tag{44}$$

$$u_n^{k+1} = u_n^k + \delta u_n^k, \quad g_n^{k+1} = g_n^k + \delta g_n^k \tag{45}$$

$$v_n^{k+1} = v_n^k + \delta v_n^k, \quad l_n^{k+1} = l_n^k + \delta l_n^k \tag{46}$$

We overlook any signs of higher-order abilities, similar to the conventional Newton-Raphson technique, leading to the equations taking on a new form;

$$\delta f_n - \delta f_{n-1} - \frac{1}{2}h_n\left(\delta p_n + \delta p_{n-1}\right) = \left(r_1\right)_n \tag{47}$$

$$\delta p_n - \delta p_{n-1} - \frac{1}{2}h_n\left(\delta q_n + \delta q_{n-1}\right) = \left(r_2\right)_n \tag{48}$$

$$\delta g_n - \delta g_{n-1} - \frac{1}{2}h_n\left(\delta v_n + \delta v_{n-1}\right) = \left(r_3\right)_n \tag{49}$$

$$\delta u_n - \delta u_{n-1} - \frac{1}{2}h_n\left(\delta v_n + \delta v_{n-1}\right) = \left(r_4\right)_n \tag{50}$$

$$\delta\theta_n - \delta\theta_{n-1} - \frac{1}{2}h_n\left(\delta l_n + \delta l_{n-1}\right) = \left(r_5\right)_n \tag{51}$$

Once again, by incorporating equations (47)-(51) into equations (38)-(42), the equations are further simplified as shown below;

$$(a_1)_n\,\delta q_n + (a_2)_n\,\delta q_{n-1} + (a_3)_n\,\delta\theta_n + (a_4)_n\,\delta\theta_{n-1} + (a_5)_n\,\delta l_n + (a_6)_n\,\delta l_{n-1} + (a_7)_n\delta p_n + (a_8)_n\delta p_{n-1} + (a_9)_n\,\delta g_n + (a_{10})_n\,\delta g_{n-1} + (a_{11})_n\delta v_n + (a_{12})_n\delta v_{n-1} = (r_6)_n \tag{52}$$

$$(b_1)_n\,\delta v_n + (b_2)_n\,\delta v_{n-1} + (b_3)_n\,\delta f_n + (b_4)_n\,\delta f_{n-1} + (b_5)_n\,\delta q_n + (b_6)_n\,\delta q_{n-1} + (b_7)_n\,\delta g_n + (b_8)_n\,\delta g_{n-1} = (r_7)_n \tag{53}$$

$$(c_1)_n\,\delta p_n + (c_2)_n\,\delta p_{n-1} + (c_3)_n\,\delta\theta_n + (c_4)_n\,\delta\theta_{n-1} + (c_5)_n\,\delta f_n + (c_6)_n\,\delta f_{n-1} + (c_7)_n\,\delta m_n + (c_8)_n\,\delta m_{n-1} = (r_8)_n \tag{54}$$

Along with boundary limits,

$$\delta f_0 = 0, \quad \delta g_0 = 0, \delta p_0 = 0, \quad \delta u_0 = 1, \quad \delta\theta_0 = 1 \tag{55}$$

$$\delta p_n = 1, \quad \delta\theta_n = 0, \quad \delta u_n = 0 \tag{56}$$

5 Matrix Form of Algebraic Equations

The subsequent crucial stage involves arranging the previously estimated equations in a matrix format. If this is executed incorrectly, either the matrix solution approach falters due to a particular matrix (determinant = 0) or submatrix, the method's efficiency greatly diminishes due to a lack of apparent configuration in the matrix. We possess:

$$A\delta = r, \tag{57}$$

$$[A] = \begin{bmatrix} \frac{[A_1][C_1]}{[B_2][A_2][C_2]} & \cdots & \cdots \\ \vdots & \ddots & \vdots \\ \vdots & \cdots & \frac{[B_{n-1}][A_{n-1}][C_{n-1}]}{[B_n][A_n]} \end{bmatrix},$$
$$[\delta] = \begin{bmatrix} [\delta_1] \\ [\delta_2] \\ \vdots \\ [\delta_{n-1}] \\ [\delta_n] \end{bmatrix}, \quad [r] = \begin{bmatrix} [r_1] \\ [r_2] \\ \vdots \\ [r_{n-1}] \\ [r_n] \end{bmatrix}, \tag{58}$$

6 Analysis and Discussion of Results

Influence of reduced gravity, temperature dependent viscosity and aligned magnetic field on flow behavior, heating efficiency and magnetic flux of magnetic fluid motion along vertical plate is explored. The nonlinear coupled model with continuity equation, flow momentum equation and magnetic flow momentum equation is developed under suitable boundary values. The porous medium effects are applied to reduced excessive heating energy and better heat transfer optimization. The appropriate stream variables and similarity variables are used to convert PDEs into ODEs for developing pertinent parameters. The numerical solution of fluid velocity, fluid temperature and magnetic velocity is deduced using Keller box scheme with central difference formula and Newton Raphson approach. The skinfriction magnitude, Nusselt quantity and magnetic flux quantity are explored in geometrical and numerical form. The main outcomes are discussed below.

Figures 2a-2c explore the fluid velocity flow, fluid temperature flow and magnetic velocity flow along vertical plate using different values of viscosity parameter $\epsilon = 1.0, 5.0, 9.0$ and 14.0. The increasing value of fluid velocity is detected as viscosity parameter decreases $\epsilon = 1.0$ in Figure 2a. For high value of viscosity parameter $\epsilon = 1.4$, the lower flow magnitude in fluid velocity is observed. In Figure 2b, the behavior of fluid temperature is discussed. The increasing flow of fluid temperature is found as viscosity parameter decreases $\epsilon = 1.0$. The decreasing flow rate of fluid temperature is observed as viscosity parameter increases $\epsilon = 1.4$. In Figure 2c, the distinct behavior of magnetic velocity is observed than other values. For high value of viscosity parameter $\epsilon = 1.4$, the increasing flow magnitude of magnetic velocity is found. For lower value of viscosity parameter $\epsilon = 1.0$, the decreasing flow magnitude of magnetic velocity is detected.

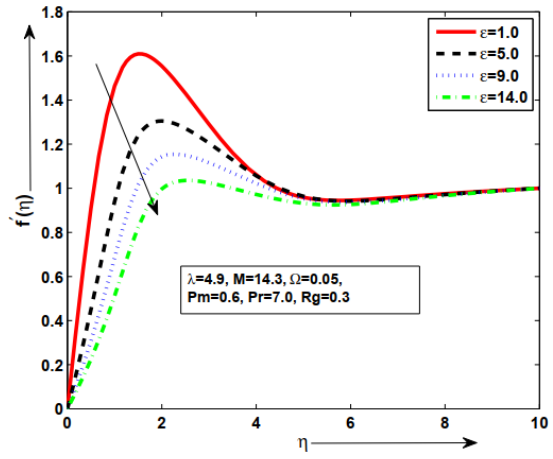

(a)

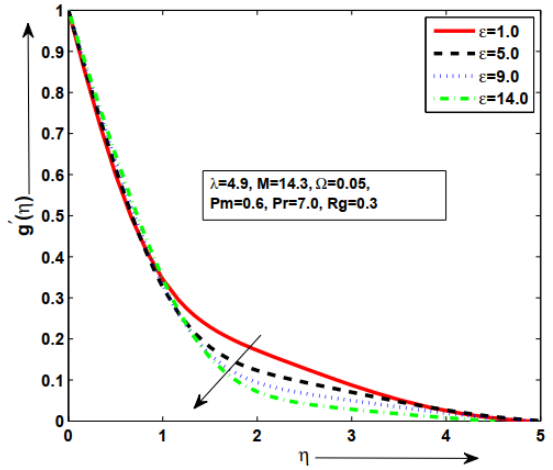

(b)

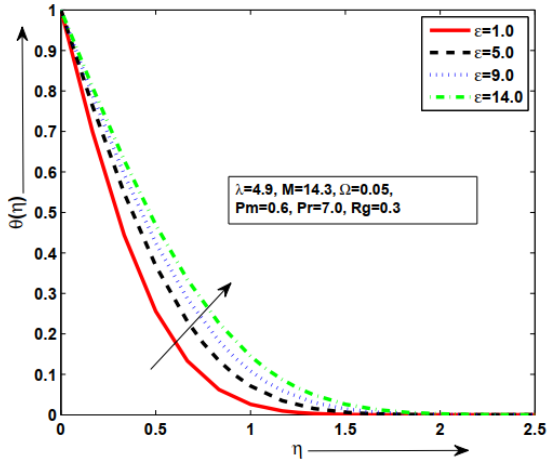

(c)

Figure 2. Pictorial representation of $f'(\eta), g'(\eta)$ and $\theta(\eta)$ for ε.

Figures 3a-3c explore the fluid velocity flow, fluid temperature flow and magnetic velocity flow along vertical plate using different values of reduced-gravity parameter $Rg = 0.1, 0.3, 0.5$ and 0.7. The increasing value of fluid velocity is detected as reduced-gravity parameter increases $Rg = 0.7$ in Figure 3a. For lower value of reduced-gravity parameter $Rg = 0.1$, the lower flow magnitude in fluid velocity is observed. In Figure 3b, the behavior of fluid temperature is discussed. The increasing flow of fluid temperature is found as reduced-gravity parameter increases $Rg = 0.7$. The decreasing flow rate of fluid temperature is observed as reduced-gravity parameter decreases $Rg = 0.1$. In Figure 3c, the distinct behavior of magnetic velocity is observed than other values. For high value of reduced-gravity parameter $Rg = 0.7$, the decreasing flow magnitude of magnetic velocity is found. For lower value of reduced-gravity parameter $Rg = 0.1$, the increasing flow magnitude of magnetic velocity is detected.

Figures 4a-4c explore the fluid velocity flow, fluid temperature flow and magnetic velocity flow along vertical plate using different values of Prandtl parameter $\mathrm{Pr} = 0.5, 1.0, 3.0$ and 7.0. The increasing value of fluid velocity is detected as Prandtl parameter decreases $\mathrm{Pr} = 0.5$ in Figure 4a. For high value of Prandtl parameter $\mathrm{Pr} = 7.0$, the lower flow magnitude in fluid velocity is observed. In Figure 4b, the behavior of fluid temperature is discussed. The increasing flow of fluid temperature is found as Prandtl parameter increases $\mathrm{Pr} = 7.0$. The decreasing flow rate of fluid temperature is observed as Prandtl parameter decreases $\mathrm{Pr} = 0.5$. In Figure 4c, the distinct behavior of magnetic velocity is observed than other values. For high value of Prandtl parameter $\mathrm{Pr} = 7.0$, the decreasing flow magnitude of magnetic velocity is found. For lower value of Prandtl parameter $\mathrm{Pr} = 0.5$, the increasing flow magnitude of magnetic velocity is detected.

Figures 5a-5c explore the fluid velocity flow, fluid temperature flow and magnetic velocity flow along vertical plate using different values of porous parameter $\Omega = 1.0, 3.0, 5.0$ and 7.0. The increasing value of fluid velocity is detected as porous parameter $\Omega = 1.0$ decreases in Figure 5a. For high value of porous parameter $\Omega = 7.0$, the lower flow magnitude in fluid velocity is observed. In Figure 5b, the behavior of fluid temperature is discussed. The increasing flow of fluid temperature is found as porous parameter $\Omega = 7.0$ increases. The decreasing flow rate of fluid temperature is observed as porous parameter $\Omega = 1.0$ decreases. In Figure 5c, the distinct behavior of magnetic velocity is observed than other values. For high value of porous parameter $\Omega = 7.0$, the increasing flow magnitude of magnetic velocity is

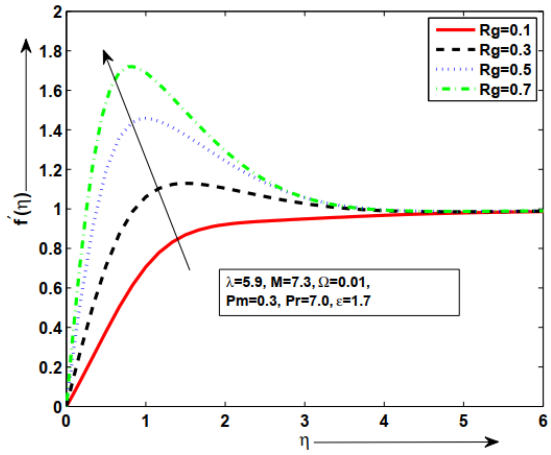

(a)

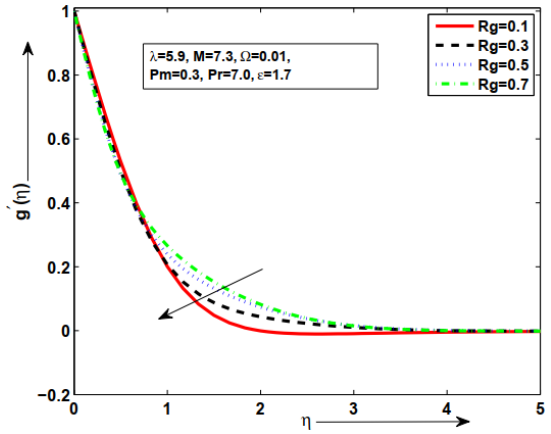

(b)

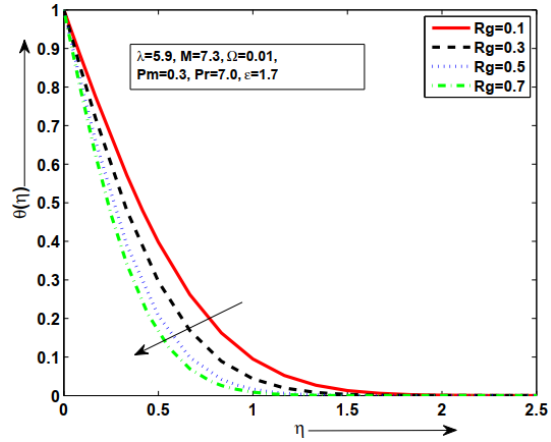

(c)

Figure 3. Pictorial representation of $f'(\eta), g'(\eta)$ and $\theta(\eta)$ for R_g.

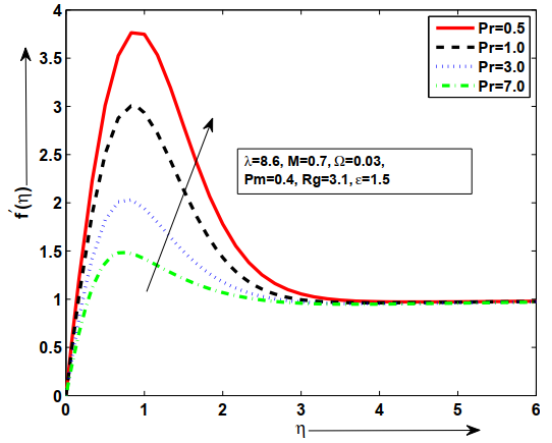

(a)

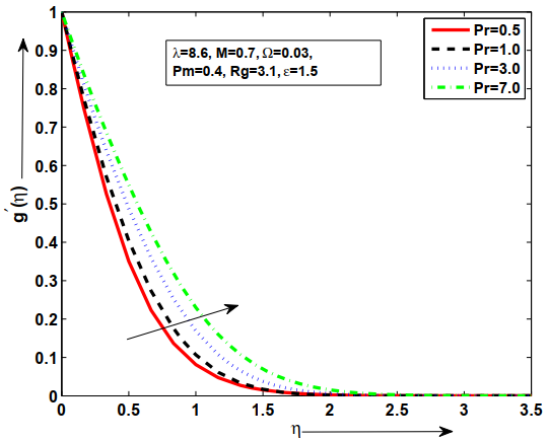

(b)

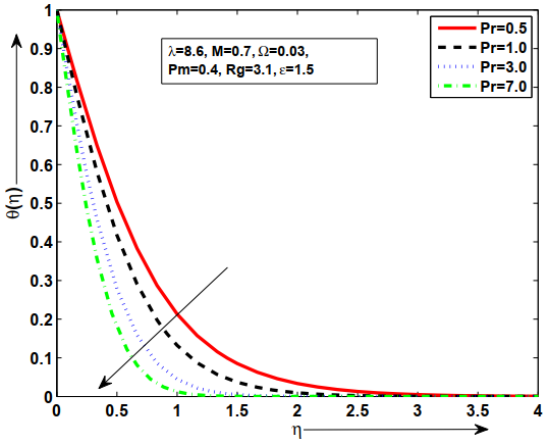

(c)

Figure 4. Pictorial representation of $f'(\eta), g'(\eta)$ and $\theta(\eta)$ for P_r.

found. For lower value of porous parameter $\Omega = 1.0$, the decreasing flow magnitude of magnetic velocity is detected.

Figures 6a-6c explore the fluid velocity flow, fluid temperature flow and magnetic velocity flow along vertical plate using different values of buoyancy parameter $\lambda = 0.1, 1.0, 3.0$ and 5.0. The increasing value of fluid velocity is detected as buoyancy parameter $\lambda = 5.0$ increases in Figure 6a. For lower value of buoyancy parameter $\lambda = 0.1$, the lower flow magnitude in fluid velocity is observed. In Figure

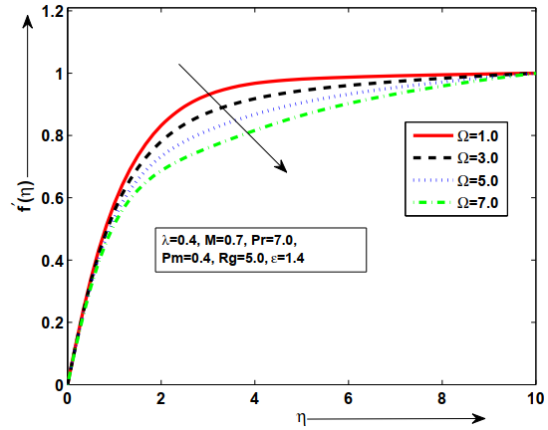

(a)

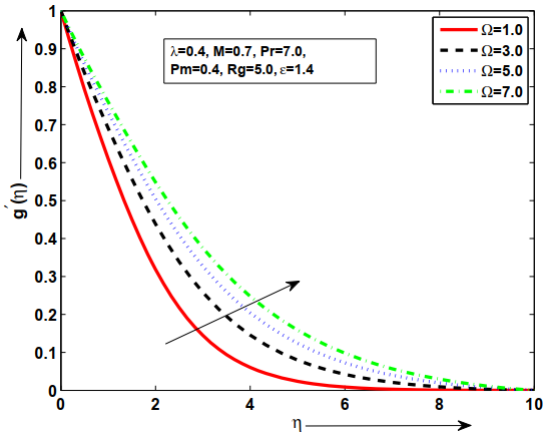

(b)

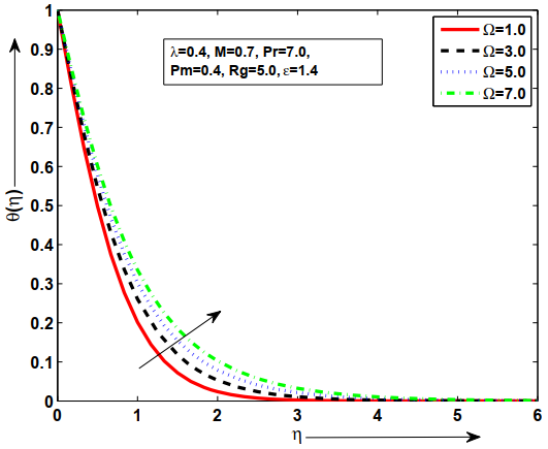

(c)

Figure 5. Pictorial representation of $f'(\eta), g'(\eta)$ and $\theta(\eta)$ for Ω.

6b, the behavior of fluid temperature is discussed. The increasing flow of fluid temperature is found as buoyancy parameter $\lambda = 0.1$ decreases. The decreasing flow rate of fluid temperature is observed as buoyancy parameter $\lambda = 5.0$ increases. In Figure 6c, the distinct behavior of magnetic velocity is observed than other values. For high value of buoyancy parameter $\lambda = 5.0$, the decreasing flow magnitude of magnetic velocity is found. For lower value of buoyancy parameter $\lambda = 0.1$, the increasing flow magnitude of magnetic velocity is detected.

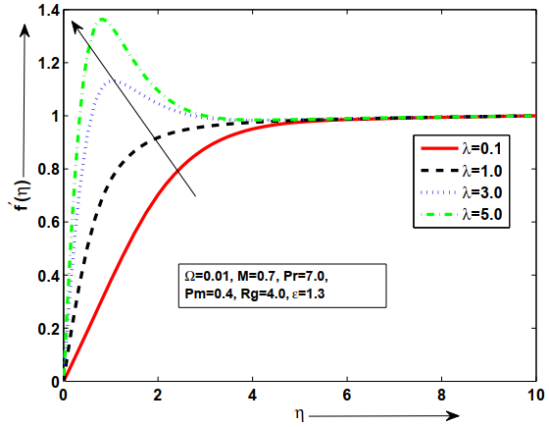

(a)

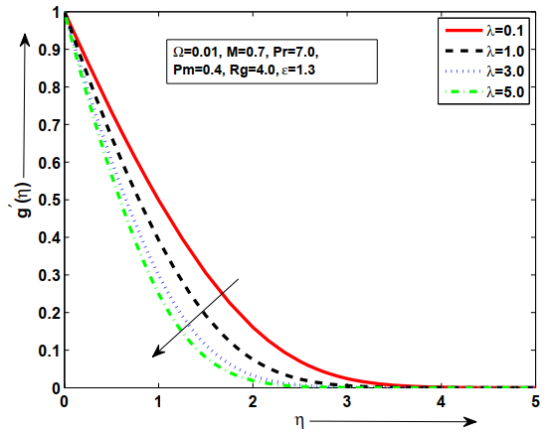

(b)

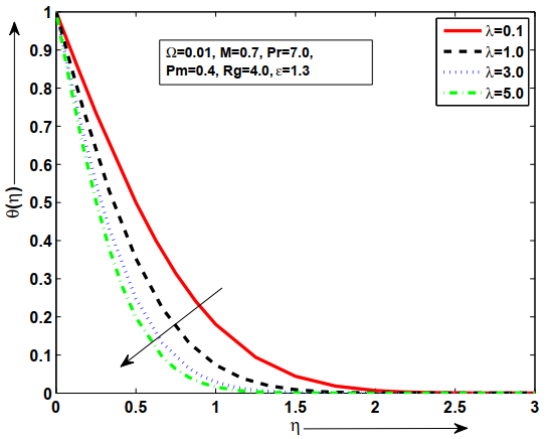

(c)

Figure 6. Pictorial representation of $f'(\eta), g'(\eta)$ and $\theta(\eta)$ for λ.

Figures 7a-7c explore the fluid velocity flow, fluid temperature flow and magnetic velocity flow along

vertical plate using different values of magnetic parameter $M = 0.1, 1.5, 3.5$ and 5.5. The increasing value of fluid velocity is detected as magnetic parameter $M = 5.5$ increases in Figure 7a. For lower value of magnetic parameter $M = 0.1$, the lower flow magnitude in fluid velocity is observed. In Figure 7b, the behavior of fluid temperature is discussed. The increasing flow of fluid temperature is found as magnetic parameter $M = 0.1$ decreases. The decreasing flow rate of fluid temperature is observed as magnetic parameter $M = 5.5$ increases. In Figure 7c, the distinct behavior of magnetic velocity is observed than other values. For high value of magnetic parameter $M = 5.5$, the decreasing flow magnitude of magnetic velocity is found. For lower value of magnetic parameter $M = 0.1$, the increasing flow magnitude of magnetic velocity is detected.

Table 1. Numerical results for $f''(0)$, $-g''(0)$ and for $-\theta'(0)$ for various values of $\varepsilon = 1.0, 5.0, 9.0, 14.0$, while other parameters are fixed.

$\varepsilon =$	$f''(0)$	$-g''(0)$	$-\theta'(0)$
1.0	1.588768829342915	0.745631051314296	1.792476247598057
5.0	0.672160340031253	0.639913472185171	1.412382098417781
9.0	0.453301366853811	0.588168142609830	1.254839314888374
14.0	0.332274641235580	0.547148464443530	1.139754658767668

Table 2. Numerical results for $f''(0)$, $-g''(0)$ and for $-\theta'(0)$ for various values of $R_g = 1.0, 2.0, 3.0, 4.0$, while other parameters are fixed.

R_g	$f''(0)$	$-g''(0)$	$-\theta'(0)$
0.1	1.094524856085405	0.381168870540422	0.727570962514822
0.3	1.231884617453011	0.579088928566133	1.079087599966608
0.5	1.369073043829710	0.704466975144494	1.313044496007767
0.7	1.495770201500889	0.804029751353085	1.502949236807803

Table 3. Comparison of skin friction $f''(0)$ for various values of magnetic force $M = 0.0, 0.1, 0.5, 1.0$ with some fixed parameters.

M	Hamad and Ferdows [32]	Alsaedi et al. [33]	Awais et al. [34]	Present Results
0.0	1.9991	1.9991	1.9991	1.9990
0.1	2.0101	2.0101	2.0101	2.0069
0.5	2.1102	2.1102	2.1102	2.0800
1.0	2.3902	2.3902	2.3902	2.1834

Table 1 illustrates the inspiration of the viscosity constraint ($\varepsilon = 1.0, 5.0, 9.0$, and 14.0) alongside the upward magneto-thermal surface to analyze the behavior of corporeal properties: skinfriction rate, magneto intensity rate, and heating energy rate of the

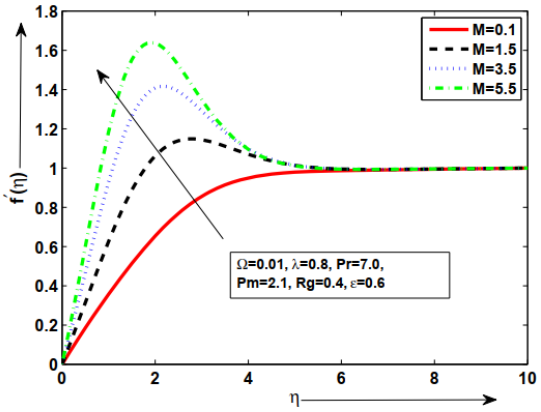

(a)

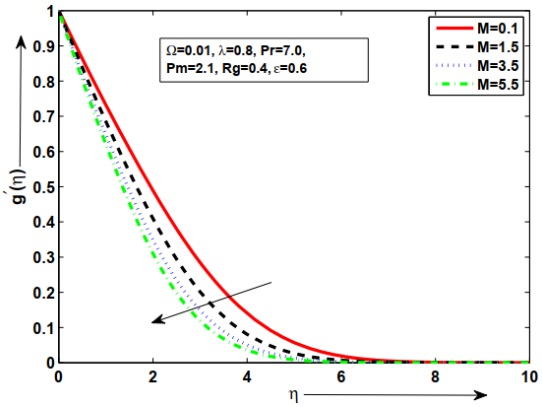

(b)

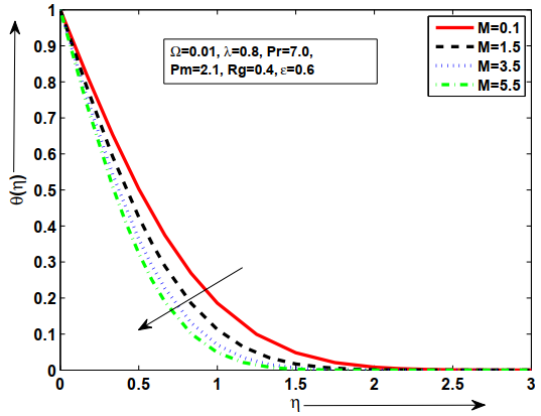

(c)

Figure 7. Pictorial representation of $f'(\eta), g'(\eta)$ and $\theta(\eta)$ for M.

fluid. The constant parameters $\mathrm{Pr} = 7.0$, $\lambda = 4.9$, and $M = 14.3$ are maintained. From Table 1, the uppermost skinfriction occurs at a lower $\varepsilon = 1.0$, whereas the smallest skin friction value is observed at a larger $\varepsilon = 14.0$. Similarly, magnetic intensity is heightened at lower $\varepsilon = 1.0$ but diminishes at higher $\varepsilon = 14.0$. Heat transfer is found to be highest at smaller $\varepsilon = 1.0$ and lowest at larger $\varepsilon = 14.0$, all under the influence of Prandtl quantity $\mathrm{Pr} = 7.0$. In Table 2,

it is presumed that maximum skinfriction occurs at larger $Rg = 0.7$, whereas minimum skinfriction is observed at lesser $Rg = 0.1$. Magnetic intensity follows a similar pattern, being highest at larger $Rg = 0.7$ and lowest at smaller $Rg = 0.1$. A correlation is noted between the reduced gravity parameter and the change in $-\theta'(0)$: as reduced gravity Rg increases, $-\theta'(0)$ also increases, and vice versa. In Table 3, a numerical comparison of skin friction with previous results is computed for different magnetic force values $(M = 0.0, 0.1, 0.5, 1.0)$. The numerical outcomes exhibit favorable agreement with the current physical model, demonstrating accuracy in the calculated skinfriction, magneto strength, and heating magnitude. These values are obtained from the velocity, magnetic field, and temperature profiles, further confirming the reliability of the present numerical analysis.

7 Conclusion

Influence of reduced gravity, temperature dependent viscosity and aligned magnetic field on flow behavior, heating efficiency and magnetic flux of magnetic fluid motion along vertical plate is explored. The nonlinear coupled model with continuity equation, flow momentum equation and magnetic flow momentum equation is developed under suitable boundary values. The porous medium effects are applied to reduced excessive heating energy and better heat transfer optimization. The appropriate stream variables and similarity variables are used to convert PDEs into ODEs for developing pertinent parameters. The numerical solution of fluid velocity, fluid temperature and magnetic velocity is deduced using Keller box scheme with central difference formula and Newton Raphson approach. The skinfriction magnitude, Nusselt quantity and magnetic flux quantity are explored in geometrical and numerical form. The core outcomes are discussed below.

- The analysis reveals that fluidvelocity plot reaches its peak at the lower ε value of 1.0, although the lowest fluidvelocity plot is observed at the larger ε value of 14.0. This trend prominently emerges in the context of reduced gravity effects.
- The magneto velocity graph exhibits a pronounced peak with a strong response at higher reduced gravity $(Rg = 0.7)$ for the liquid characterized by $\lambda = 5.9$ and $\mathrm{Pr} = 7.0$, eventually approaching an asymptotic behavior as per the specified condition
- The analysis indicates that the temperature distribution demonstrates a peak performance at a minor MHD Prandtl quantity $(Pm = 0.1)$, while the slightest temperature charge is observed at a upper Pm value of 2.5.
- The highest skinfriction is observed at the slighter charge of $\varepsilon = 1.0$, while the lowest skinfriction value is identified at the superior value of $\varepsilon = 14.0$.
- It is concluded that the magneto strength reaches its supreme at the lower ε value of 1.0, whereas a lower magnetic intensity is evident at the higher ε value of 14.0.
- The analysis reveals that heat transfer is at its peak when ε is smaller $(\varepsilon = 1.0)$, although the smallest heat transfer charge is observed at greater ε values $(\varepsilon = 14.0)$, influenced by the Prandtl number.

Data Availability Statement

Data will be made available on request.

Funding

This work was supported without any funding.

Conflicts of Interest

The authors declare no conflicts of interest.

Ethical Approval and Consent to Participate

Not applicable.

References

[1] Kay, A., Kuiken, H. K., & Merkin, J. H. (1995). Boundary-layer analysis of the thermal bar. *Journal of fluid mechanics, 303*, 253-278. [Crossref]

[2] Hazarika, G. C., & Ch, U. S. G. (2012). Effects of variable viscosity and thermal conductivity on MHD flow past a vertical plate. *Matematicas: Ensenanza Universitaria, 20*(2), 45-54.

[3] Srinivasacharya, D., Mallikarjuna, B., & Bhuvanavijaya, R. (2016). Effects of thermophoresis and variable properties on mixed convection along a vertical wavy surface in a fluid saturated porous medium. *Alexandria Engineering Journal, 55*(2), 1243-1253. [Crossref]

[4] Gbadeyan, J. A., Titiloye, E. O., & Adeosun, A. T. (2020). Effect of variable thermal conductivity and viscosity on Casson nanofluid flow with convective heating and velocity slip. *Heliyon, 6*(1). [Crossref]

[5] Chin, K. E., Nazar, R., Arifin, N. M., & Pop, I. (2007). Effect of variable viscosity on mixed convection

boundary layer flow over a vertical surface embedded in a porous medium. *International Communications in Heat and Mass Transfer, 34*(4), 464-473. [Crossref]

[6] Mahmoud, M. A. A. (2013). Effects of chemical reaction and heat generation on double-diffusive natural convection along a non-isothermal vertical cone in non-Newtonian fluid saturated porous medium with variable viscosity and thermal radiation. *Latin American applied research, 43*(2), 107-112.

[7] Malik, M. Y., Jamil, H., Salahuddin, T., Bilal, S., Rehman, K. U., & Mustafa, Z. (2016). Mixed convection dissipative viscous fluid flow over a rotating cone by way of variable viscosity and thermal conductivity. *Results in physics, 6*, 1126-1135. [Crossref]

[8] Elaiw, A. M., Bakr, A. A., & Ibrahim, F. S. (2012). Effect of variable viscosity on vortex instability of non-Darcy free convection boundary layer flow adjacent to a non-isothermal horizontal surface in a porous medium. *Boundary Value Problems, 2012*(1), 26. [Crossref]

[9] Hazarika, G. C., & Konch, J. (2014). Effects of Variable viscosity and thermal conductivity on MHD free convective flow along a vertical porous plate with viscous dissipation. *International Journal of Mathematics Trends and Technology-IJMTT, 15*. [Crossref]

[10] Lin, C. R., & Chen, C. O. K. (1993). Free convection flow from a vertical isothermal cone with temperature-dependent viscosity. *Polymer-Plastics Technology and Engineering, 32*(4), 277-287. [Crossref]

[11] Kishan, N., & Amrutha, P. (2015). Variable viscosity effects on mixed convection heat and mass transfer along a semi-infinite vertical plate in the presence of chemical reaction and viscous dissipation. *International Journal of Engineering, Science and Technology, 7*(2), 27-42. [Crossref]

[12] Pullepu, B., Sambath, P., Selva Rani, M., Chamkha, A. J., & Viswanathan, K. K. (2015). Numerical solutions of free convective flow from a vertical cone with mass transfer under the influence of chemical reaction and heat generation/absorption in the presence of UWT/UWC. *Journal of Applied Fluid Mechanics, 9*(1), 343-356. [Crossref]

[13] Abbas, A., & Ashraf, M. (2020). Combined effects of variable viscosity and thermophoretic transportation on mixed convection flow around the surface of a sphere. *Thermal Science, 24*(6 Part B), 4089-4101. [Crossref]

[14] Umavathi, J. C., Chamkha, A. J., & Mohiuddin, S. (2016). Combined effect of variable viscosity and thermal conductivity on free convection flow of a viscous fluid in a vertical channel. *International Journal of Numerical Methods for Heat & Fluid Flow, 26*(1), 18-39. [Crossref]

[15] Pullepu, B., Sambath, P., & Viswanathan, K. K. (2014). Effects of chemical reactions on unsteady free convective and mass transfer flow from a vertical cone with heat generation/absorption in the presence of VWT/VWC. *Mathematical Problems in Engineering, 2014*(1), 849570. [Crossref]

[16] Palani, G., Lalith Kumar, E. J., & Kim, K. Y. (2016). Free convection effects on a vertical cone with variable viscosity and thermal conductivity. *Journal of Applied Mechanics and Technical Physics, 57*(3), 473-482. [Crossref]

[17] Reddy, M. G., Dinesh, P. A., & Sandeep, N. (2017, November). Effects of variable viscosity and porosity of fluid, Soret and Dufour mixed double diffusive convective flow over an accelerating surface. In *IOP conference series: materials science and engineering* (Vol. 263, No. 6, p. 062012). IOP Publishing. [Crossref]

[18] Awasthi, B. (2018). Effects of heat and mass flux on MHD free convection flow through a porous medium with radiation and first order chemical reaction. *International Journal of Applied Mechanics and Engineering, 23*(4). [Crossref]

[19] Srinivasacharya, D., Mallikarjuna, B., & Bhuvanavijaya, R. (2015). Radiation effect on mixed convection over a vertical wavy surface in Darcy porous medium with variable properties. *Journal of Applied Science and Engineering, 18*(3), 265-274. [Crossref]

[20] Sehra, Haq, S. U., Shah, S. I. A., Nisar, K. S., Jan, S. U., & Khan, I. (2021). Convection heat mass transfer and MHD flow over a vertical plate with chemical reaction, arbitrary shear stress and exponential heating. *Scientific reports, 11*(1), 4265. [Crossref]

[21] Ganji, D. D., Mahboobtosi, M., Jalili, B., & Jalili, P. (2024). Heat transfer analysis of magnetized fluid flow through a vertical channel with thin porous surfaces: Python approach. *Case Studies in Thermal Engineering, 60*, 104643. [Crossref]

[22] Niranjana, N., Vidhya, M., Govindarajan, A., Siva, E. P., & Priyadarshini, E. (2019, June). Mass transfer effects on flow over a vertical plate oscillating in porous plate in the presence of transverse magnetic field. In *AIP Conference Proceedings* (Vol. 2112, No. 1, p. 020106). AIP Publishing LLC. [Crossref]

[23] Cheng, C. Y. (1999). Effect of a magnetic field on heat and mass transfer by natural convection from vertical surfaces in porous media-an integral approach. *International communications in heat and mass transfer, 26*(7), 935-943. [Crossref]

[24] Onanuga, O. K., Chendo, M. A. C., & Erusiafe, N. E. (2018). Thermal Radiation of Hydromagnetic Stagnation Gravity-Driven Flow through a Porous Confined Cylinder with Non-Uniform Heat Source. *Open Journal of Fluid Dynamics, 8*(4), 361-377. [Crossref]

[25] Srinivasulu, T., & Goud, B. S. (2021). Effect of inclined magnetic field on flow, heat and mass transfer of Williamson nanofluid over a stretching sheet. *Case*

Studies in Thermal Engineering, 23, 100819. [Crossref]

[26] Bayones, F. S., Abd-Alla, A. M., & Thabet, E. N. (2021). Effect of heat and mass transfer and magnetic field on peristaltic flow of a fractional Maxwell fluid in a tube. *Complexity, 2021*(1), 9911820. [Crossref]

[27] Lotto, M. A., Johnson, K. M., Nie, C. W., & Klaus, D. M. (2017). The impact of reduced gravity on free convective heat transfer from a finite, flat, vertical plate. *Microgravity Science and Technology, 29*(5), 371-379. [Crossref]

[28] Ostrach, S. (1982). Convection phenomena at reduced gravity of importance in space processing of materials. *Bulletin of Materials Science, 4*(2), 109-123. [Crossref]

[29] Awwad, F. A., Ismail, E. A., & Gul, T. (2023). Heat and mass transfer gravity driven fluid flow over a symmetrically-vertical plane through neural networks. *Symmetry, 15*(6), 1288. [Crossref]

[30] Maranna, T., Sneha, K. N., Mahabaleshwar, U. S., Sarris, I. E., & Karakasidis, T. E. (2022). An effect of radiation and MHD Newtonian fluid over a stretching/shrinking sheet with CNTs and mass transpiration. *Applied Sciences, 12*(11), 5466. [Crossref]

[31] Mabood, F., Fatunmbi, E. O., Benos, L., & Sarris, I. E. (2022). Entropy generation in the magnetohydrodynamic Jeffrey nanofluid flow over a stretching sheet with wide range of engineering application parameters. *International Journal of Applied and Computational Mathematics, 8*(3), 98. [Crossref]

[32] Hamad, M. A. A., & Ferdows, M. (2012). Similarity solution of boundary layer stagnation-point flow towards a heated porous stretching sheet saturated with a nanofluid with heat absorption/generation and suction/blowing: a Lie group analysis. *Communications in Nonlinear Science and Numerical Simulation, 17*(1), 132-140. [Crossref]

[33] Alsaedi, A., Awais, M., & Hayat, T. (2012). Effects of heat generation/absorption on stagnation point flow of nanofluid over a surface with convective boundary conditions. *Communications in Nonlinear Science and Numerical Simulation, 17*(11), 4210-4223. [Crossref]

[34] Awais, M., Hayat, T., Ali, A., & Irum, S. (2016). Velocity, thermal and concentration slip effects on a magneto-hydrodynamic nanofluid flow. *Alexandria Engineering Journal, 55*(3), 2107-2114. [Crossref]

[35] Arshad, M., Alharbi, F. M., Hassan, A., Haider, Q., Alhushaybari, A., Eldin, S. M., ... & Galal, A. M. (2023). Effect of inclined magnetic field on radiative heat and mass transfer in chemically reactive hybrid nanofluid flow due to dual stretching. *Scientific Reports, 13*(1), 7828. [Crossref]

[36] Wang, C., Rong, D., Zhang, W., Gong, B., & Wu, J. (2023). The flow and heat transfer performances of magnetic nanofluid in a duct in presence of magnetic fields with different direction. *Journal of Mechanical Science and Technology, 37*(9), 4899-4909. [Crossref]

[37] Abdelhafez, M. A., Abd-Alla, A. M., Abo-Dahab, S. M., & Elmhedy, Y. (2023). Influence of an inclined magnetic field and heat and mass transfer on the peristaltic flow of blood in an asymmetric channel. *Scientific Reports, 13*(1), 5749. [Crossref]

Dr. Zia Ullah received the PhD degree in Mathematics with field computational fluid dynamics and heat transfer from University of Sargodha, Sargodha 40100, Pakistan, in 2022. He is working as an Assistant Professor in department of mathematics, University of Lahore, Sargodha Campus, Pakistan. He is now working as Postdoctoral Researcher in Harbin Institute of Technology, Shenzhen, China. He has published several scientific research articles in well reputed international journals. He has several years of teaching and research experience. (Email: ziakhan6009@gmail.com)

Amir Abbas received the PhD degree in Mathematics from University of Sargodha, Sargodha 40100, Pakistan, in 2021. (Email: amir.abbas@bgnu.edu.pk)

Uzma Tariq received the Master degree in Mathematics from University of Lahore, Sargodha-Campus, Sargodha 40100, Pakistan, in 2024. (Email: uzmatariq472@gmail.com)

Malik Izhar Ul Haq received the Master degree in Mathematics from University of Lahore, Sargodha-Campus, Sargodha 40100, Pakistan, in 2024. (Email: maliksaggu594@gmail.com)

Alishba Kaynat received the Master degree in Mathematics from University of Lahore, Sargodha-Campus, Sargodha 40100, Pakistan, in 2024. (Email: alishbakaynat@gmail.com)

Anila Bibi received the Master degree in Mathematics from University of Lahore, Sargodha-Campus, Sargodha 40100, Pakistan, in 2024. (Email: anilashabir60@gmail.com)

Tehreem Soha received the Master degree in Mathematics from University of Lahore, Sargodha-Campus, Sargodha 40100, Pakistan, in 2024. (Email: tehreemsoha@gmail.com)

M Waheed Iqbal received the Master degree in Mathematics from University of Lahore, Sargodha-Campus, Sargodha 40100, Pakistan, in 2024. (Email: waheediqbal6495@gmail.com)

Muhammad Ashraf received the Master degree in Mathematics from University of Lahore, Sargodha-Campus, Sargodha 40100, Pakistan, in 2024. (Email: ashrafmuhammad806@gmail.com)